JB
Journals.ASM.org

Influence of the AgrC-AgrA Complex on the Response Time of *Staphylococcus aureus* Quorum Sensing

Sandeep K. Srivastava, Kalagiri Rajasree, Aneesa Fasim, Gayathri Arakere, Balasubramanian Gopal

Molecular Biophysics Unit, Indian Institute of Science, Bangalore, India

The *Staphylococcus aureus agr* quorum-sensing system plays a major role in the transition from the persistent to the virulent phenotype. *S. aureus agr* type I to IV strains are characterized by mutations in the sensor domain of the histidine kinase AgrC and differences in the sequences of the secreted autoinducing peptides (AIP). Here we demonstrate that interactions between the cytosolic domain of AgrC ($AgrC_{Cyto}$) and the response regulator domain of AgrA ($AgrA_{RR}$) dictate the spontaneity of the cellular response to AIP stimuli. The crystal structure of $AgrC_{Cyto}$ provided a basis for a mechanistic model of AgrC-AgrA interactions. This model enabled an analysis of the biochemical and biophysical parameters of AgrC-AgrA interactions in the context of the conformational features of the AgrC-AgrA complex. This analysis revealed distinct sequence and conformational features that determine the affinity, specificity, and kinetics of the phosphotransfer reaction. This step, which governs the response time for transcriptional reengineering triggered by an AIP stimulus, is independent of the *agr* type and similar for agonist and antagonist stimuli. These experimental data could serve as a basis on which to validate simulations of the quorum-sensing response and for strategies that employ the *agr* quorum-sensing system to combat biofilm formation in *S. aureus* infections.

Multiple pore-forming toxins, immune evasion factors, and adhesins contribute to acute and chronic *Staphylococcus aureus* infections in humans (1). The expression of most of these virulence factors is controlled by the accessory gene regulator (*agr*), a two-component regulatory system in *S. aureus* (2). The sequence composition of the autoinducing peptide (AIP) with a five-member thiolactone ring provides a basis on which to distinguish between different *S. aureus* strains, also referred to as *agr* types I to IV. The interaction of the AIP with AgrC, a membrane-bound histidine kinase, regulates the catalytic activity of AgrC. Mutations in AgrC across *S. aureus* strains of different *agr* types are confined to the ectodomain. This observation is consistent with experimental data that suggest that the signal recognition mechanism is confined to the extracellular and membrane-associated components (3). The subsequent steps of signal transduction involve phosphorylation of AgrA by AgrC, followed by the interaction of phosphorylated AgrA with cognate promoters to trigger *agr*-dependent reengineering of the transcriptional profile. This step incorporates signal amplification due to AgrA-induced expression from the P2 promoter and expression of RNAIII, a downstream effector that regulates the expression of virulence factors and other transcriptional regulators (4). Prominent changes in the transcriptional profile induced by AgrA include the expression of the characterized immune response suppressors α and β phenol-soluble modulins (5). The production and secretion of the AIPs involve the action of the permease AgrB on the AgrD propeptide (6).

The sensor module of AgrC (residues 1 to 205) contains six membrane-spanning helices. The cytoplasmic histidine kinase component (residues 206 to 430) has two subdomains—a membrane-proximal dimerization and histidine phosphotransfer (DHp) subdomain and the catalytic and ATP binding (CA) subdomain to which it is flexibly connected (7). AgrC is a dimeric protein and is activated by *trans* autophosphorylation upon the recognition of an AIP stimulus (8). AgrA has two domains. The response regulator domain of AgrA (residues 1 to 130; $AgrA_{RR}$ here) is connected with the DNA binding domain (residues 147 to 238) by a flexible linker. The transient nature of AgrC-AgrA interactions is a significant barrier to obtaining a structural model that can explain AIP-dependent transcriptional regulation. Thus, despite extensive biochemical characterization, the conformational rearrangements leading to autophosphorylation of AgrC and the subsequent phosphotransfer to AgrA remain unclear. The temporal variations in these steps of intracellular signal transduction are relevant, as AgrC-AgrA interactions are also governed by changes in the cellular concentrations of these proteins induced by AIP stimuli. The crystal structure of the catalytic domain of AgrC provided a template for a mechanistic model by which to rationalize the initial steps of intracellular signal transduction. This model and the biochemical characteristics of the AgrC-AgrA interactions reveal details of the intracellular signal transduction mechanism in *S. aureus* that ensures temporal fidelity in the cellular response to a quorum-sensing stimulus.

MATERIALS AND METHODS

***S. aureus* strains.** *S. aureus* methicillin-sensitive clinical isolates of all of the types, i.e., 559 (*agr* type I), 1437 (*agr* type II), 1039 (*agr* type III), and 368 (*agr* type IV) (9), were obtained from an *S. aureus* repository maintained by Gayathri Arakere. The *agr* null mutant (RN6911) was used as a reference strain in this study (10). The *agr* types of these strains were confirmed by multiplex *agr* typing (11) and sequencing of *agr* operon genes (data not shown).

Cloning, expression, and purification of recombinant cytosolic AgrC and AgrA. Several PCR primers were designed to obtain expression constructs for AgrC [$AgrC_{FL}$, $AgrC_{Cyto}$, and $AgrC_{(234-430)}$] and

Received 4 February 2014 Accepted 16 May 2014
Published ahead of print 23 May 2014
Address correspondence to Balasubramanian Gopal, bgopal@mbu.iisc.ernet.in.
S.K.S., K.R., and A.F. contributed equally to this work.
Supplemental material for this article may be found at http://dx.doi.org/10.1128/JB.01530-14.

doi:10.1128/JB.01530-14

AgrA (the entire protein is also referred to as $AgrA_{FL}$, and the response regulator is referred to as $AgrA_{RR}$) in the pET expression vectors pET28a and pET22b (Novagen, Inc.). Site-directed mutagenesis of $AgrC_{Cyto}$ ($AgrC_{Cyto}$Y251W) was performed with partially overlapping primers. These AgrC and AgrA constructs (see Table SA1 in the supplemental material) contained a hexahistidine tag at either the N or the C terminus and could be overexpressed in *Escherichia coli* Rosetta(DE3)pLysS cells (Novagen) at 20°C upon induction with 0.5 mM isopropyl-β-D-thiogalactopyranoside (Gold Biotechnology, Inc.). All protein samples were purified by nickel-agarose affinity chromatography (Ni-IDA; GE Healthcare), followed by gel filtration chromatography (HiPrep 16/60 Sephacryl S-200; GE Healthcare). Fractions containing the target protein were loaded onto a gel filtration column equilibrated with 20 mM Tris-HCl (pH 8.5)–200 mM NaCl–5% glycerol. The proteins were eluted from the column and concentrated to up to 10 mg/ml in the case of $AgrC_{Cyto}$ and to up to 1 to 2 mg/ml in the cases of $AgrA_{FL}$ and $AgrA_{RR}$.

***In vitro* phosphorylation of AgrC.** Autophosphorylation of $AgrC_{Cyto}$ was examined as described previously (12), with minor modifications. Briefly, purified $AgrC_{Cyto}$ (1 to 2 μM) was preequilibrated in 50 mM Tris-HCl (pH 7.2)–50 mM KCl–5 mM $MgCl_2$ in a final reaction volume of 100 μl for 10 min at 25°C. The autophosphorylation reaction was initiated by adding aliquots (5, 15, 25, 100, and 300 μM) of [γ-^{32}P]ATP (specific activity, 2,500 Ci/mmol; BRIT, Hyderabad, India). Twelve-microliter aliquots were removed at different times (1, 10, 20, 30, 40, 50, 80, 100 and 300 s), and the reaction was quenched by the addition of 5× SDS sample buffer (2.5% SDS, 25% glycerol, 125 mM Tris-HCl [pH 6.8], 200 mM dithiothreitol, 0.0025% bromphenol blue). Samples were analyzed without heating by 12.5% SDS-PAGE. The gels were dried and subjected to autoradiography. These experiments were repeated in triplicate, and the extent of phosphorylation was analyzed by phosphorimaging. The intensities were plotted against time, allowing the rates of phosphorylation to be calculated as initial rates from the progress curves. The amount of phosphorylated $AgrC_{Cyto}$ ($AgrC_{Cyto}$~P) was quantified by using a standard curve generated with known concentrations of [γ-^{32}P]ATP. Initial rates were calculated from linear regression plots of [$AgrC_{Cyto}$~P] versus time. The kinetic parameters (K_m and K_{cat}) (12–15) were obtained by fitting the kinetic profile with a nonlinear regression program (GraphPad Prism).

Phosphotransfer between $AgrC_{Cyto}$ and AgrA. Phosphorylation of $AgrC_{Cyto}$ was performed as described earlier. The excess [γ-^{32}P]ATP was removed with a microspin column (Millipore, Inc.). Five micromolar phosphorylated $AgrC_{Cyto}$ was added to 15 μM $AgrA_{FL}$ and 15 μM $AgrA_{RR}$ in phosphorylation buffer (50 mM Tris [pH 7.2], 100 mM KCl, 5 mM $MgCl_2$). The reaction mixture was incubated at 25°C, and samples (12 μl) were removed at different times, quenched with 3 μl of 5× SDS sample buffer, and visualized by 15% SDS-PAGE. The phosphorylated protein was visualized by phosphorimaging. A plot of the recorded intensities against time was used to determine the rate constants of kinase activity.

Quaternary structure of $AgrC_{Cyto}$ and $AgrA_{FL}$. The quaternary association of these proteins was analyzed by size exclusion chromatography (Superdex 200-10/300GL; GE Healthcare). The concentration of $AgrC_{Cyto}$ used for size exclusion chromatography was ca. 40 μM. These experiments were also performed in the presence of 2 mM Mg-ATP. Size exclusion chromatography of $AgrA_{FL}$ (ca. 40 μM) was also performed without a phosphate donor, as well as in the presence of 10 mM acetyl phosphate. Dynamic light scattering (DLS) experiments were performed at 20°C on a Viscotek-802 DLS instrument. The concentration of $AgrC_{Cyto}$ was varied from 0.25 to 2.5 mg/ml, whereas $AgrA_{FL}$ was used at 0.7 to 2.5 mg/ml in these experiments. The $AgrC_{Cyto}$ protein was in 20 mM HEPES (pH 7.5)–200 mM NaCl, while $AgrA_{FL}$ was in 20 mM HEPES (pH 7.5)–500 mM NaCl–10% glycerol. A phosphate donor (acetyl phosphate) was used to obtain phosphorylated AgrA. The data were analyzed with Omnisize 3.0 software.

Crystallization and structure determination. Initial screening for crystallization conditions was performed with Hampton and Molecular Dimension screens with different expression constructs of the cytosolic domain of AgrC. Crystals of the sensor kinase domain of AgrC could be obtained from the $AgrC_{Cyto}$ construct at 20°C by the microbatch method (1:1 paraffin and silicone oil mixture; Hampton Research, Inc.). A drop containing 1 μl of protein solution (15-mg/ml concentration) and 1 μl of a solution containing 0.2 M ammonium acetate, 0.1 M trisodium citrate dihydrate (pH 6.0), 36% 2-methyl-2,4-pentanediol, and 200 mM sodium potassium tartrate yielded crystals with dimensions of 0.3 by 0.3 by 0.2 mm in 3 to 4 weeks. The crystals were flash frozen in liquid nitrogen for data collection at 100K. Although different ligands [Mg-ATP and the ATP analogues adenylyl imidodiphosphate and adenylyl (β,γ-methylene) diphosphate] were used for cocrystallization with AgrC constructs, these crystals could not be improved.

AgrC crystals diffracted up to 2.2Å at a synchrotron source (BM14 beam line at the European Synchrotron Radiation Facility, Grenoble, France). The images were processed with iMOSFLM (16) and scaled with SCALA (17). Phase information was obtained by molecular replacement with the sensor histidine kinase of *Thermotoga maritima* (Protein Data Bank [PDB] code 2C2A) as a search model with Phaser (18), and the initial model was built with Buccaneer (19). The model was refined with Refmac5 from the CCP4 suite of programs (20), and the fit of the model to the electron density was examined with Coot (21). The topology and parameter files for ligands were generated with the PRODRG server (22). The model was validated with PROCHECK (23). All of the figures illustrating this molecule were prepared with PyMOL (Schrödinger, LLC).

Molecular modeling and docking of $AgrA_{RR}$ on $AgrC_{Cyto}$. The crystal structure of the cytosolic domain of AgrC formed the basis of the construction of a model of AgrC ($AgrC_{FL}$). This involved modeling of the dimerization domain that precedes the ATP binding domain of AgrC. This hybrid model formed the basis for a dimer of $AgrC_{Cyto}$ (with the RosettaDock suite) and was aided by a comparison with the *T. maritima* HK853 structure (PDB code 3DGE). The model of $AgrA_{RR}$ was obtained from the Phyre server, which used *Salmonella enterica* serovar Typhimurium CheB (PDB code 1A2O) as a template.

Fluorescence studies. Fluorescence studies of $AgrC_{Cyto}$ and $AgrA_{FL}$ were performed on a Jasco FP6300 fluorimeter at 25°C. The spectrum of the denatured protein was obtained by incubating the $AgrC_{Cyto}$Y251W protein sample in 8 M urea. In these control experiments, 5 μM $AgrC_{Cyto}$Y251W mutant was incubated in a buffer containing 8 M urea, 20 mM HEPES (pH 7.5), and 200 mM NaCl for 30 min. The excitation wavelength was set to 280 nm with a slit width of 2.5 nm, while the emission spectrum was recorded from 300 to 400 nm at a slit width of 10 nm. Each recording was an average of three scans. An identical experiment was performed with 4 μM $AgrA_{FL}$. The kinetics of the association of $AgrC_{Cyto}$Y251W with $AgrA_{FL}$ was examined by steady-state fluorescence with excitation at 280 nm and the emission wavelength set at 344 nm. In these experiments, 0 to 80 μM $AgrA_{FL}$ was titrated against 4 μM $AgrC_{Cyto}$Y251W in 20 mM HEPES (pH 7.5)–200 mM NaCl–10 mM $MgCl_2$–5% glycerol. The fraction of $AgrA_{FL}$ titrated against $AgrC_{Cyto}$Y251W [$F(x)$] was calculated with the equation $F(x) = [Y(x) - Y_{unbound}]/(Y_{bound} - Y_{unbound})$, where $Y(x)$ is the fluorescence signal of $AgrC_{Cyto}$Y251W at an $AgrA_{FL}$ concentration of x, $Y_{unbound}$ is the fluorescence signal of the protein in the absence of $AgrA_{FL}$, and Y_{bound} is the fluorescence signal of the protein at saturating concentrations of the $AgrA_{FL}$ protein. The fraction bound was analyzed with the ligand binding nonlinear regression equation (GraphPad prism software) $F(x) = Y(x) + [a/(a \times c)]$, where $F(x)$ is the fraction of $AgrC_{Cyto}$Y251W titrated against $AgrA_{FL}$, $Y(x)$ is the maximum fraction of $AgrC_{Cyto}$Y251W in $AgrA_{FL}$, a is the dissociation constant (K_d) of the AgrC-AgrA complex, and c is the concentration (μM) of $AgrA_{FL}$.

SPR spectroscopy experiments. The kinetics of the interaction between $AgrC_{Cyto}$ and AgrA was examined by surface plasmon resonance (SPR) spectroscopy (BIACORE 2000; GE Healthcare). The purified $AgrA_{FL}$ or $AgrA_{RR}$ protein was immobilized on a CM5 chip (BIACORE; GE Healthcare) at a surface density of 12 ng/mm^2. Various concentrations

of $AgrC_{Cyto}$ were the analytes in these experiments. The first panel of the CM5 chip served as a control. SPR spectroscopy experiments were performed with 50 mM HEPES buffer (pH 7.5), 150 mM NaCl, 10 mM $MgCl_2$, and 5% glycerol. These experiments were also repeated in the presence of 2 mM ATP. Similar experiments were performed with $AgrC_{Cyto}$Y251W as an analyte. Binding constants were obtained with the BIAevaluation software (BIACORE; GE Healthcare). This software determines the association and dissociation constants of the analyte (A) and ligand (B) by fitting experimental data to a 1:1 interaction model. The rate of complex formation during analyte injection is given by $d[AB]/dt = k_a[A][B] - k_d[AB]$, where k_a and k_d are the association and dissociation rate constants. The dissociation rate of the ligand-analyte complex at the end of the injection is $d[AB]/dt = -k_d[AB]$. If the total ligand (B) is assumed to be involved in complex formation (measured in response units, then the rate equation can be written as $dR/dt = k_aCR_{max} - (k_aC + k_d)R$. An important assumption is the steady state, wherein the net rate of complex formation becomes zero: $k_aCR_{max} = (k_aC + k_d)R$. Setting $R = R_{eq}$ (the equilibrium response level) and expressing k_a/k_d as equilibrium association constants results in the final equation $R_{eq} = (K_ACR_{max})/(K_AC + 1)$. A plot of R_{eq} against the analyte concentration (C) provides an estimate of K_A. The inverse of K_A, the equilibrium dissociation constant (K_D), is reported here.

qRT-PCR analysis of AIP-induced activation and inhibition. For monitoring of the activation of the *agr* regulon, RNA was isolated from *S. aureus* cultures (24). Cells were harvested at the 1-, 3-, 5-, and 7-h time points; suspended at 1:2 in RNA-Later reagent (Qiagen); and further incubated at room temperature for 5 to 10 min before centrifugation and storage at −80°C. To study AIP-induced inhibition, all *agr* (I, II, III, and IV)-type cultures were grown overnight. The culture supernatants were subsequently passed through 0.2-μm filters as described earlier (24). Each *agr*-type isolate was grown for 3 h before adding the cross-inhibiting culture supernatant (from the other three *S. aureus agr* types) in a 1:1 ratio and grown further for 4 h at 37°C. Cells were harvested at the 5- and 7-h time points after the addition of supernatants. Samples were resuspended in 200 μl of buffer containing 3,000 μg of lysozyme, 6 μg of lysostaphin, and 10 μg of proteinase K in Tris-EDTA buffer (30 mM Tris-HCl [pH 8.0], 1 mM EDTA). RNA was isolated with the RNeasy minikit (Qiagen). One microgram of RNA was converted to cDNA with the QuantiTect reverse transcription kit (Qiagen). Twenty nanograms of cDNA per reaction was used for quantitative real-time PCR (qRT-PCR) with the Bio-Rad iQ5 system. The primers used to amplify target genes are listed in Table SA2 in the supplemental material. Gyrase A (*gyrA*) was used as the internal control. The relative transcriptional levels of target genes were determined by the $2^{-\Delta\Delta CT}$ method (25) by using the values from the 1-h time point as a control for activation and those from the 3-h time point as a control for inhibition experiments.

Hemolysin assays. The protocol for the hemolysin assays was adapted from that of Sakoulas et al. (26). *S. aureus* cultures grown in tryptic soy broth (TSB) were streaked perpendicular to the RN4220 strain on sheep blood agar (SBA) plates and incubated at 37°C for 24 h and then at 4°C for 24 h to trigger a cold shock response. To inhibit hemolysis, overnight cultures were inoculated at a 1:1,000 dilution and grown for 3 h before cross-inhibiting supernatants were added to the cultures and they were grown further for 4 h. Five percent SBA plates were overlaid with 2 ml of lyophilized (20× concentrated) and filter-sterilized supernatants. When the plates were dry, the strains were streaked onto plates containing cross-inhibiting supernatants and incubated at 37°C.

Immunoprecipitation of AgrA from *S. aureus* lysates. AgrA pulldown assays were performed with antibodies raised against AgrA in rabbits. Cell pellets from 50-ml *S. aureus* cultures of each *agr* type were grown and suspended in 3 ml of lysis buffer (50 mM Tris [pH 7.5], 150 mM NaCl, 1 mM $MgCl_2$, 0.1 mM EDTA, 0.1 mM EGTA, 0.1 mM NaF, 0.1 mM Na_3VO_4, 0.5 mM phenylmethylsulfonyl fluoride, 200 μg/ml lysozyme, 0.1 mg/ml lysostaphin, 20 μg/ml DNase, 10 μg/ml RNase, 15 μg/ml protease cocktail inhibitor) for 30 min at room temperature. The lysates were centrifuged at 7,000 rpm for 10 min at 4°C, and the supernatants were subsequently ultracentrifuged at 60,000 rpm for 50 min at 4°C to collect the cytosolic fractions. Five milligrams of lysate at each time point was incubated with 20 μl of *N*-hydroxysuccinimide (NHS)-activated Sepharose beads coupled to AgrA antibodies for 30 min at 4°C and washed with lysis buffer (50 mM Tris [pH 7.9], 150 mM NaCl, 1 mM $MgCl_2$ 0.1 mM EDTA, 0.1 mM EGTA, 0.1 mM NaF, 0.1 mM Na_3VO_4) before elution with 15 μl of 2 M NaCl. The eluates were separated by 15% SDS-PAGE, electroblotted onto a polyvinylidene difluoride membrane, and probed with AgrA primary antibodies (1:1,000) and horseradish peroxidase-labeled goat anti-rabbit IgG (1:3,000) secondary antibodies. Immunoblots were developed with ECL (enhanced-chemiluminescence) reagent (Biosource).

TABLE 1 Diffraction data and refinement statistics

Parameter	Value[d]
Diffraction data	
Wavelength (Å)	0.97895
Resolution range (Å)	34.81–2.2
Unit cell parameters (Å)	67.3, 67.37, 101.99
Space group	$P4_32_12$
Total no. of reflections	355,542 (31,207)
No. of unique reflections	12,556 (1,080)
Completeness (%)	100 (100)
Multiplicity	28.3 (28.9)
Wilson B factor (Å^2)	30.8
R_{merge} (%)[a]	10.5 (67.4)
$<I/\sigma(I)>$	23.1 (6.1)
Refinement	
R_{cryst} (%)[b]	19.6
R_{free} (%)[c]	22.5
No. of residues	148
No. of solvents	55
No. of ligands	5
B factors (Å^2)	
Protein	42.77
Water	62.91
Ligand	70.51
RMS deviations in bond:	
Length (Å)	0.0065
Angle (°)	1.137
Model Ramachandran plot	
Favored region (%)	95.83
Allowed region (%)	4.17
Outliers (%)	0

[a] $R_{merge} = \Sigma_{hkl}\Sigma_i|I_i(hkl) - <I(hkl)>|/\Sigma_{hkl}\Sigma_i I_i(hkl)$, where $I_i(hkl)$ is the intensity of the ith reflection and $<I(hkl)>$ is the average intensity.
[b] $R_{cryst} = \Sigma_{hkl}|F_{obs}| - |F_{calc}|/\Sigma_{hkl}|F_{obs}|$.
[c] R_{free} was calculated the same way as R_{cryst} but by using 5% of the data that were excluded from the refinement calculation.
[d] The values in parentheses are for the outer shell.

RESULTS

Crystal structure of the cytosolic domain of AgrC. Extensive screening of recombinant protein constructs (see Table SA1 in the supplemental material) with various lengths yielded diffraction quality crystals of $AgrC_{Cyto}$. The data collection and refinement statistics are compiled in Table 1. The phase information for this structure was obtained by molecular replacement with the *T. maritima* sensor kinase (PDB code 2C2A) as a search model (27).

Analysis of the diffraction data and subsequent biochemical analyses of $AgrC_{Cyto}$ crystals suggested that these crystals contained an 18-kDa fragment of $AgrC_{Cyto}$, perhaps because of *in situ* proteolysis in the crystallization drop. While we were successful in crystallizing the intact cytosolic domain in the case of another AgrC construct [$AgrC_{(234-430)}$], these crystals diffracted to a lower resolution (see Fig. SA1 and Table SA3 in the supplemental material). Also, the polypeptide stretch corresponding to the dimerization helix and the catalytic histidine residue (His-239) could not be modeled in the experimental maps because of poor electron density. The subsequent structural description is thus restricted to the CA domain of $AgrC_{Cyto}$.

The CA domain (residues 278 to 430) of $AgrC_{Cyto}$ has a six-stranded β-sheet (β1 to β6) stacked against four helices (α1 to α4) (Fig. 1A). This domain is broadly similar to the ATP binding domains of proteins belonging to the GHKL superfamily of ATPases including TM0853 (PDB code 2C2A), PrrB (PDB code 1YS3), DesK (PDB code 3EHG), CheA (PDB code 1I59), and PhoQ (PDB code 1ID0) (28). However, in the ATP binding domain of AgrC, the β1 strand is part of a β-sheet formed with five other β strands. This differs from other reported structures, wherein the first β strand of the ATP binding domain forms a linker between the dimerization and ATP binding domains. This β-sheet forms the back wall of the ATP binding cavity. The polypeptide that covers the nucleotide binding pocket, also referred to as the ATP lid, is tethered between two hydrophobic clusters (27). Sequence and structural comparisons reveal that AgrC has a shorter lid in the ATP binding pocket than other characterized ATP binding domains. In the conformation seen in $AgrC_{Cyto}$, helices α3 and α4 are located at the entrance of active site. The positioning of these helices is likely to hinder substrate binding. The orientation of these helices is different from other substrate-bound ATP binding domains (for example, PDB code 2C2A) (Fig. 1B; see Fig. SA2 in the supplemental material) (27) as well as the apo domain structures (PDB code 1YS3). In this context, it is worth noting that although $AgrC_{Cyto}$ could be crystallized only in the presence of ATP, the experimental maps did not reveal electron density for ATP.

Autophosphorylation of AgrC. A time course reaction with $AgrC_{Cyto}$ in the presence of different concentrations of [γ-^{32}P]ATP at 25°C suggested a first-order reaction for the first 5 min, followed by a saturation phase over the next 20 min (Fig. 2A). The phosphorylated protein was stable for more than 1 h at 25°C (Fig. 2B). At the initial stage, the autophosphorylation reaction is first order in ATP and the dependence of k_{obs} on the ATP concentration was half maximal, at 40 ± 2 μM (K_{ATP}). The overall apparent pseudo-first-order rate of autophosphorylation, K_{cat} (K_{phos}) is 0.11 ± 0.002 min^{-1}, which is similar to that of other histidine kinases, such as *S. aureus* WalK (13), *Streptococcus pneumoniae* WalK (29), *Bacillus subtilis* NarQ (30), and *S. aureus* VraS (31).

Phosphotransfer kinetics. Incubation of $AgrC_{Cyto}$~P with AgrA revealed a rapid transfer of the phosphoryl group to AgrA (Fig. 2C); indeed, 50% of the phosphoryl group was transferred within a minute of the initiation of the reaction. A 3-fold excess of AgrA was maintained in these phosphotransfer experiments. The estimated pseudo-first-order rate constant of the phosphotransfer during the initial period at room temperature is 0.068 ± 0.001s^{-1}. The phosphotransfer kinetics support the hypothesis that transmembrane signal transduction is almost instantaneous, involving low affinity, transient AgrC-AgrA interactions. The rapid phosphotransfer is also consistent with a recent study that suggests that rapid phosphotransfer rates can be correlated with histidine kinase response regulator specificity and governs fidelity in two-component systems (32, 33). As hypothesized by the molecular model, these interactions involve only the receiver domain of AgrA. Indeed, the phosphotransfer from $AgrC_{Cyto}$~P to a shorter construct of AgrA containing only the receiver domain ($AgrA_{RR}$) is similar to that of $AgrA_{FL}$ (Fig. 2D).

$AgrC_{Cyto}$-$AgrA_{RR}$ interactions. The crystal structure of $AgrC_{Cyto}$ provided a basis for a mechanistic model of the $AgrC_{Cyto}$-$AgrA_{RR}$ complex. In this model, the arrangement of the $AgrC_{Cyto}$ dimer was modeled on *T. maritima* HK853 (PDB code 3DGE) (34, 35) (Fig. 3A). The response regulator was subsequently placed by *in silico* docking trials with the RosettaDock suite (36). In this structural arrangement, $AgrA_{RR}$ is stacked on the dimerization helices of AgrC (Fig. 3A). This model is consistent with both the conformational constraints for phosphotransfer and the observation that the interaction between a shorter construct of $AgrC_{Cyto}$ (containing only the ATP binding domain) with AgrA reduces drastically irrespective of ATP concentrations (data not shown). The molecular model of the complex thus incorporates the finding that both subdomains of $AgrC_{Cyto}$ are required for AgrA interactions and the C-terminal DNA binding domain of AgrA does not directly interact with $AgrC_{Cyto}$. The discrimination between cognate and noncognate response regulator interactions is governed by the sequence and structural features at the interface between the histidine kinase and response regulator (32, 34). The AgrC-AgrA interface suggested distinct sequence characteristics that dictate the interaction specificity in this complex (see Fig. SA3 and SA4 in the supplemental material). Several hydrophobic residues from AgrC are involved in AgrA interactions. These include Val242, Ile244, Leu245, and Leu248 in the polypeptide stretch that extends beyond Tyr251. The segments of AgrA that interact with AgrC, on the other hand, incorporate polypeptide segments on either side of Asp59. While these are conserved in AgrA types I to IV, substantial variations are seen in other response regulators. The influence of these sequence variations on specificity was experimentally examined with two noncognate response regulators, VraR and LytR (see Fig. SA5 in the supplemental material). The interaction between AgrC and these two response regulators was examined by SPR spectroscopy. Assays to evaluate the phosphotransfer between AgrC and these two noncognate response regulators were also conducted by using the same procedure adopted for the cognate AgrC-AgrA complex. The poor binding affinity and kinetics of phosphotransfer between AgrC and these two response regulators are consistent with the notion that sequence features enforce specificity in AgrC-AgrA interactions.

The extent of the interaction interface between AgrC and AgrA in the molecular model was also examined by fluorescence spectroscopy. There are no tryptophan residues in either AgrC or AgrA. The introduction of a tryptophan residue at the $AgrC_{Cyto}$-$AgrA_{RR}$ interface thus provided a strategy by which to examine AgrC-AgrA interactions by fluorescence spectroscopy. The catalytic histidine residue (His-239) in AgrC is located in one of the dimerization helices. On the basis of the $AgrC_{Cyto}$-$AgrA_{RR}$ complex model, Tyr-251, located on the same helix as His-239, was mutated to Trp (see Fig. SA6 in the supplemental material). The far UV circular dichroism spectrum of the $AgrC_{Cyto}$Y251W mutant was similar to that of $AgrC_{Cyto}$ (see Fig. SA7 in the supplemental material). We note that introduction of the tryptophan residue near the catalytic histidine did not substantially alter the

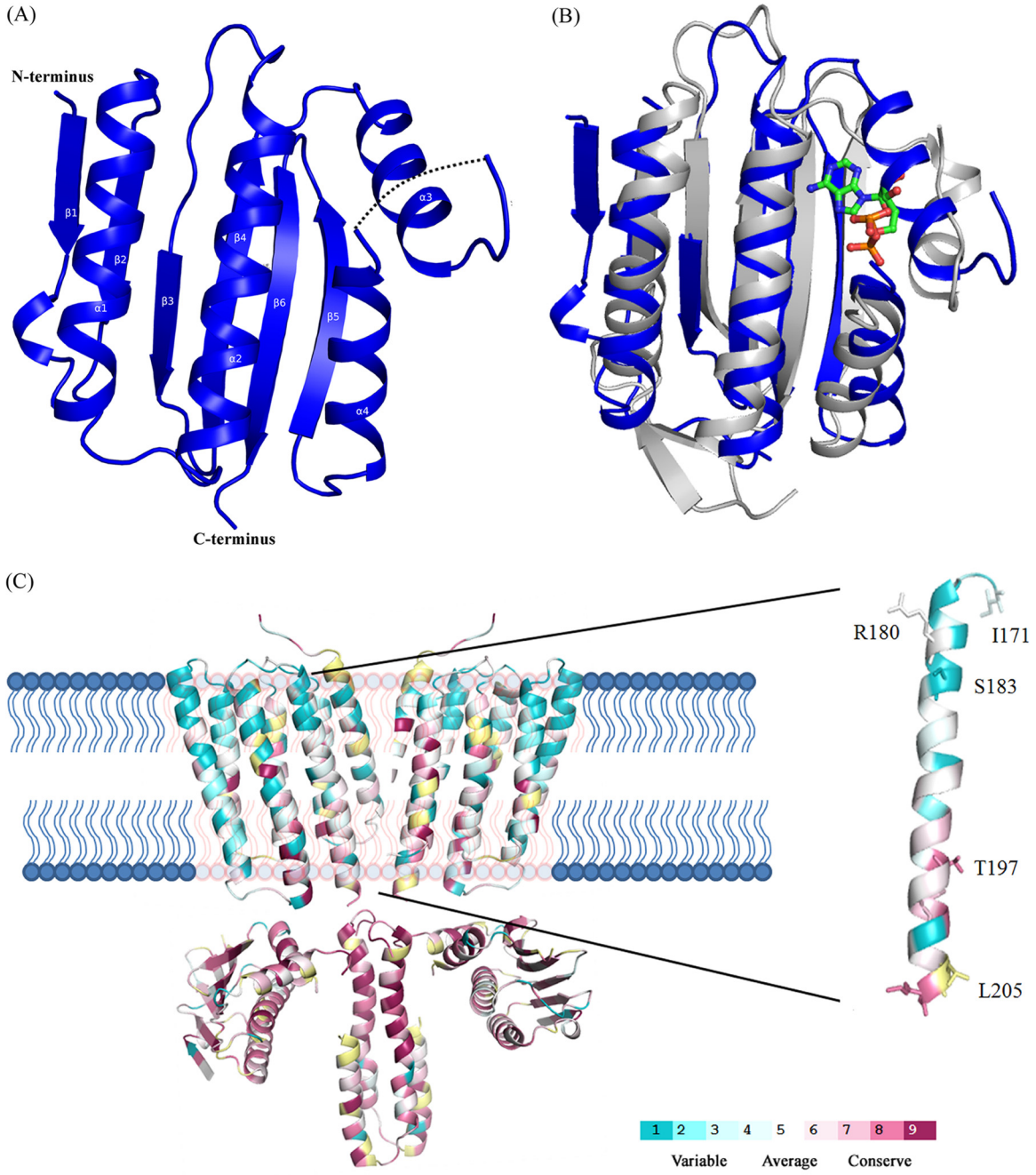

FIG 1 Conformational features of AgrC. (A) The ATP binding domain in the crystal structure of AgrC (PDB code 4BXI). Residues 389 to 393 could not be modeled in the electron density map (shown by a discontinuous line). (B) Structural superimposition of the ATP binding domain of AgrC and a representative ligand-bound ATP binding domain (TM0853; PDB code 2C2A; in gray). The lid of the ATP binding site adopts a conformation in AgrC that is different from that in other characterized domain structures in the apo- and ATP-bound forms. (C) AgrC sequence conservation across staphylococci. For this representation of sequence conservation on a structural model, the transmembrane segment of AgrC (residues 1 to 206) was modeled by using *Acetabularia acetabulum* rhodopsin AR2 (PDB code 3AM6) as a template in the LOMETS program (51). Mutations in the seventh transmembrane helix (inset) result in loss of specificity to self-activating peptides (3). The dimerization domain (residues 206 to 278) was modeled on the basis of *T. maritima* HK853 (PDB code 3DGE) by using the Phyre server (56). This figure was generated with ConSurf (52).

phosphotransfer kinetics (see Fig. SA8 in the supplemental material) or binding affinity, as estimated by SPR spectroscopy (see Fig. SA9 in the supplemental material). The fluorescence spectrum of the $AgrC_{Cyto}$Y251W mutant protein showed an emission maximum at 344 nm (Fig. 3D). A titration involving various concentrations of $AgrA_{FL}$ (0 to 80 μM) against 4 μM $AgrC_{Cyto}$Y251W was performed. Fluorescence emission was monitored at 344 nm. Fluorescence intensity saturation could be achieved by the addition of 60 μM $AgrA_{FL}$ (Fig. 3E). The K_d for the $AgrC_{Cyto}$Y251W-$AgrA_{FL}$ interaction was estimated to be 20.62 ± 2.98 μM, and that in the

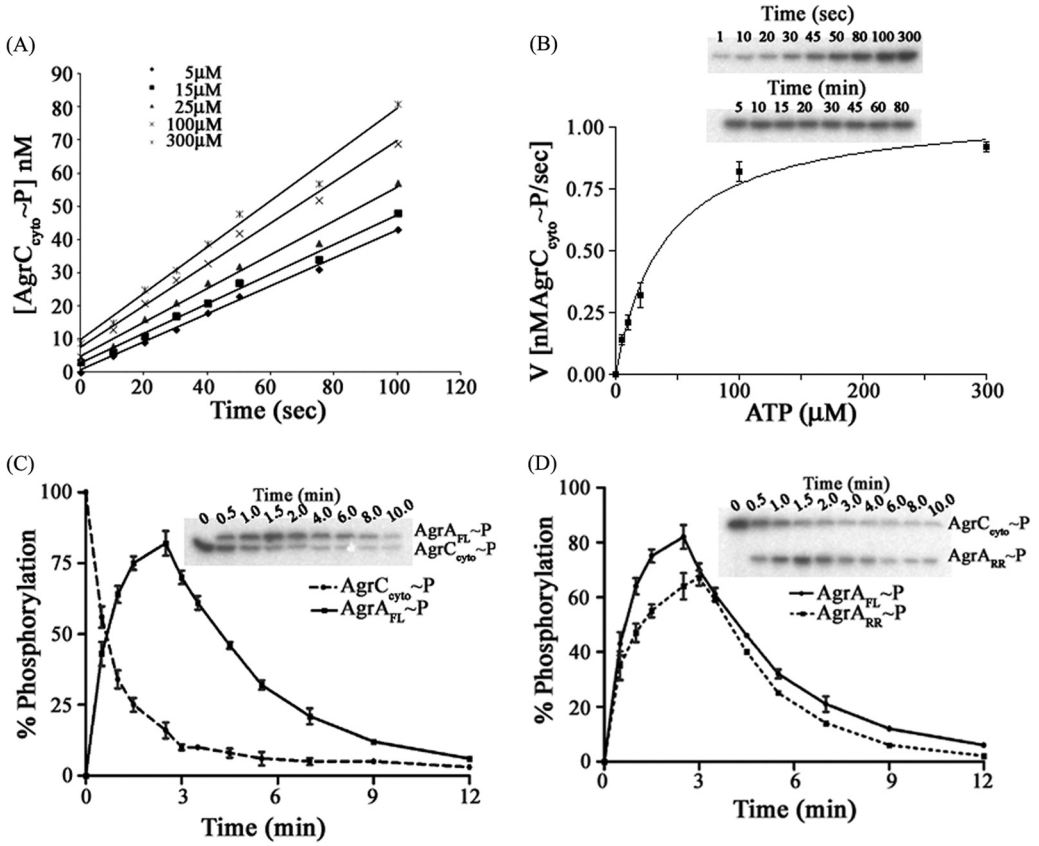

FIG 2 Kinetic parameters of phosphorylation and phosphotransfer. (A) The time course reaction used to calculate the initial rates of $AgrC_{Cyto}$~P formation at different ATP concentrations. (B) Reaction velocity-versus-[ATP] curve for AgrC autophosphorylation. The kinetic parameters of this reaction are reported in the text. (C) Data used to calculate the kinetic parameters of the phosphotransfer reaction between $AgrC_{Cyto}$ and $AgrA_{FL}$. (D) Comparison of phosphotransfer to $AgrA_{RR}$ and phosphotransfer to $AgrA_{FL}$. The error bars represent standard deviations of five independent measurements.

presence of 2 mM ATP was estimated to be 9.02 ± 2.0 μM. While these interaction parameters also suggest that ATP influences AgrC-AgrA interactions, the differences between the binding affinities derived by fluorescence spectroscopy with the SPR spectroscopy-derived parameters are likely due to differences in buffer composition.

Influence of ATP on $AgrC_{Cyto}$-$AgrA_{RR}$ interactions. SPR spectroscopy experiments were performed to evaluate the interaction between $AgrC_{Cyto}$ and AgrA (both $AgrA_{FL}$ and $AgrA_{RR}$) with and without ATP. Phosphorylation governs AgrC-AgrA interactions. We note that the interaction between $AgrC_{Cyto}$ and $AgrA_{FL}$ (K_D of 0.35 μM) is influenced by the presence of ATP (K_D of 0.15 μM) (Fig. 3B and C and Table 2). Identical measurements with the AgrA response regulator ($AgrA_{RR}$) revealed a similar change upon the addition of ATP (involving a change in the K_D from 0.91 to 0.53 μM; Table 2; see Fig. SA10 in the supplemental material). These results are consistent with the model of the complex described earlier, which suggests that $AgrA_{RR}$ dominates $AgrC_{Cyto}$-AgrA interactions. SPR spectroscopy experiments were also performed by immobilizing $AgrC_{Cyto}$ on a CM5 chip. In these experiments, different concentrations of $AgrA_{FL}$ were used as analytes. The K_D of 0.19 μM for $AgrC_{Cyto}$-$AgrA_{FL}$ interactions in this experiment is similar to that observed with immobilized $AgrA_{FL}$ (see Fig. SA11 in the supplemental material).

Phosphorylation induces AgrA dimerization. *In vivo* studies of AgrC suggested that AIP interaction does not influence the dimerization of $AgrC_{Cyto}$, whereas *trans* autophosphorylation is AIP stimulus dependent (8) (also reproduced in this study; see Fig. SA12 in the supplemental material). Upon phosphorylation, AgrC transfers the phosphate to the response regulator AgrA, which triggers downstream signal transduction. The oligomeric status of AgrA and changes in the quaternary arrangement of AgrA upon phosphorylation were examined by size exclusion chromatography and DLS experiments. $AgrA_{FL}$ is predominantly a monomer with a small dimeric component. The effect of phosphorylation on AgrA was examined by incubating this protein with 10 mM acetyl phosphate. *In vitro* phosphorylation of the response regulator by acetyl phosphate has proven to be immensely useful in dissecting the signal transduction mechanism in bacterial two-component systems. Indeed, acetyl phosphate-induced phosphorylation of AgrA revealed that phosphorylation influences the promoter specificity of AgrA (37). In this study, we noted that phosphorylation changes the oligomeric association of AgrA. The elution profile of $AgrA_{FL}$ in the presence of 10 mM acetyl phosphate revealed that most of the monomeric species were converted into the dimeric form. The mass spectrometric data on the eluted protein also suggest that 10 mM acetyl phosphate is sufficient to phosphorylate AgrA (see Fig. SA13 in the supplemental material). This finding of phosphorylation-induced dimerization was also confirmed by DLS experiments (Fig. 4).

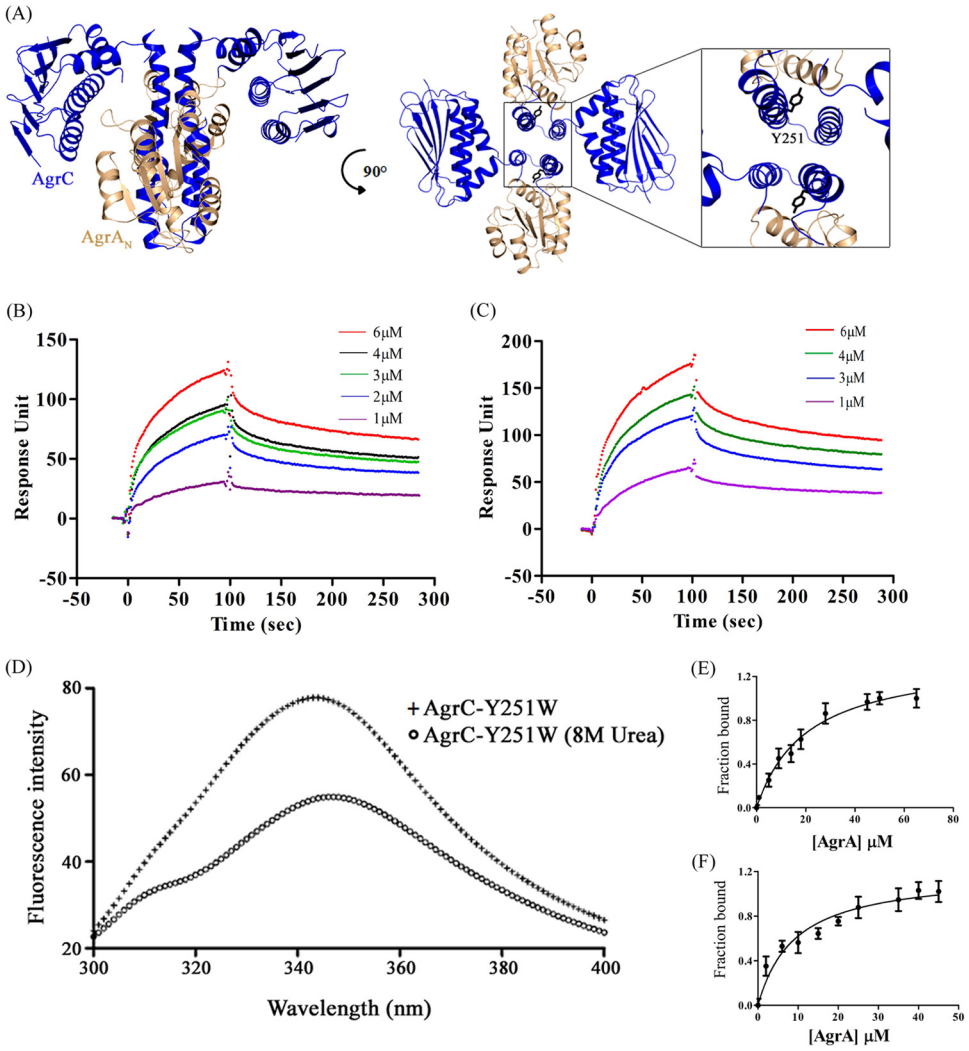

FIG 3 Phosphorylation influences AgrC$_{Cyto}$-AgrA interactions. (A) Model of AgrC$_{Cyto}$-AgrA$_{RR}$ interaction. The interacting residues in AgrC$_{Cyto}$ and AgrA are shown in more detail in Fig. SA3, SA4, and SA5 in the supplemental material. (B) SPR spectroscopy experiments were performed by immobilizing AgrA$_{FL}$ on a CM5 chip. Different concentrations of AgrC$_{Cyto}$ were used as analytes. (C) AgrC$_{Cyto}$-AgrA$_{FL}$ interactions in the presence of 2 mM ATP. (D) To quantify AgrC-AgrA interactions, Tyr-251 at the interface of AgrC and AgrA (inset highlighted in panel A) of AgrC$_{Cyto}$ was mutated to a tryptophan residue. The emission spectrum (300 to 400 nm) of AgrC$_{Cyto}$Y251W (5 μM) suggests that the tryptophan fluorescence is sensitive to the conformation of AgrC$_{Cyto}$. (E) To monitor the interaction of AgrC with AgrA, 4 μM AgrC$_{Cyto}$Y251W was titrated with increasing concentrations of AgrA$_{FL}$ (0 to 80 μM) and fluorescence emission at 344 nm was monitored (estimated K_d, 20.62 ± 2.98 μM). (F) ATP influences AgrC$_{Cyto}$-AgrA interactions. Fluorescence titration in the presence of 2 mM ATP resulted in a K_d of 9.02 ± 2.0 μM (error bars represent standard deviations; $n = 6$).

Transcriptional and phenotypic responses to AIP stimuli. The correlation between the expression of genes in the AgrA regulon and the cellular levels of AgrA was examined. This formed the basis for the evaluation of changes in the expression of genes in the *agr* regulon in different *S. aureus agr* types in the presence of agonist and antagonist AIPs. qRT-PCR for selected genes in the *agr* regulon was performed at different phases of *S. aureus* growth. The *S. aureus* growth curve suggests that the time points of 3, 5, and 7 h correspond to the early exponential, exponential, and postexponential phases of *S. aureus* growth (1). RNA was isolated at these time points, and 1 μg of RNA was converted to cDNA for quantitative PCR analysis. The expression of these genes differed among the four clinical isolates. However, in all of the cases, we noted that *agrA* expression was induced by 3 h and peaked thereafter. This pattern of induction was strongly correlated with the expression of *agrC* and less so with *agrB* (data not shown). The expression of *agrD* also followed a similar profile, where the level decreased by 7 h (Fig. 5A).

The protein levels of AgrA from *S. aureus* cell lysates was esti-

TABLE 2 Parameters of AgrC$_{Cyto}$ interaction with AgrA obtained from SPR spectroscopy

Analyte	Avg concn(10^{-7} M) ± SD	
	AgrA$_{FL}$	AgrA$_{RR}$
AgrC$_{Cyto}$	3.54 ± 0.39	9.15 ± 3.11
AgrC$_{Cyto}$ + ATP	1.54 ± 0.45	5.28 ± 1.02
AgrC$_{Cyto}$Y251W	1.26 ± 0.44	3.04 ± 0.87
AgrC$_{Cyto}$Y251W + ATP	0.81 ± 0.27	1.20 ± 0.53

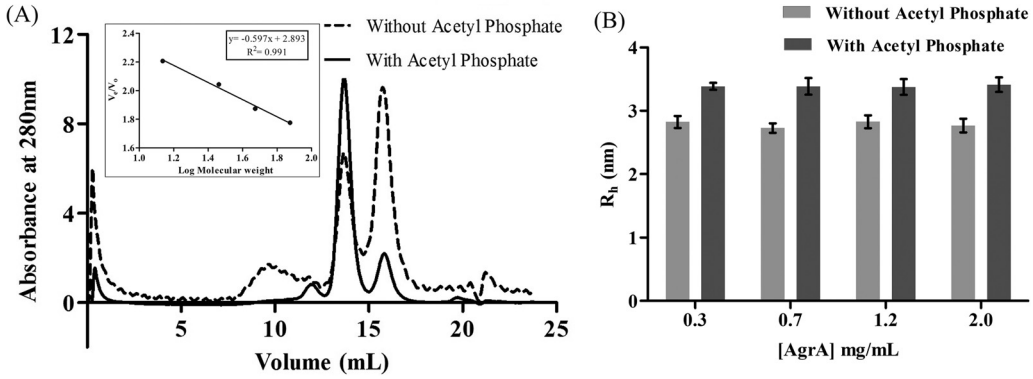

FIG 4 Quaternary association of $AgrA_{FL}$. (A) Phosphorylated $AgrA_{FL}$ is a dimer in solution. Shown is the size exclusion profile of $AgrA_{FL}$ on a Superdex 200-10/300GL column (GE Healthcare) (calibration shown in the inset). Phosphorylated AgrA was obtained by incubating this protein in 10 mM acetyl phosphate. (B) DLS measurements performed at different concentrations (0.3 to 2.0 μM) of $AgrA_{FL}$ in the presence or absence of acetyl phosphate are consistent with the size exclusion results. The error bars represent the standard deviations of three measurements with different protein preparations.

mated by immunoprecipitation at different time points and was consistent with qRT-PCR analysis. The protein level peaked at 5 h (exponential phase; Fig. 5A) and decreased thereafter in all of the clinical strains examined in this study (see Fig. SA14 in the supplemental material). This finding suggests that degradation of AgrA is not likely to influence the amplification step of the quorum-sensing response. The levels of exotoxins and surface binding proteins could also be correlated with the expression level of *agrA*. We noted that RNAIII (δ-hemolysin) levels were induced by 3 h and increased rapidly thereafter (Fig. 5A). The expression level was highest at 5 h in all of the strains and increased further in strains 559 (*agr* type I), 368 (*agr* type IV), and 1039 (*agr* type III). The α-hemolysin (*hla*) levels in strain 1437 were low compared with those of RNAIII, a finding that is consistent with the observations on *S. aureus* 772 (38) (Fig. 5A). The expression of surface binding proteins like protein A (*spa*) is also consistent with earlier reports that *spa* levels were inversely correlated with the expression of genes in the *agr* operon (Fig. 5A) (39). These observations were also examined by using an *agr* null strain (RN6911). A comparison of the expression levels of RNAIII and *spa* in *agr* type I (559) and *agr* null (RN6911) strains revealed that AgrA dominates RNAIII expression and thereby *Hla* levels, whereas *spa* levels remain unaffected (see Fig. SA15 in the supplemental material). In the case of AIP-induced inhibition, we note that the expression of all of the genes examined was downregulated in a similar time frame (less than 2 h) by antagonistic AIP stimuli (Fig. 5B; see Fig. SA16 in the supplemental material). Put together, the expression analysis results revealed that temporal fidelity in AIP-induced transcriptional responses is independent of the *S. aureus agr* type. Furthermore, AgrA degradation does not appear to influence intracellular signal transduction.

Hemolysin assays were performed to examine the time taken for secreted toxins to manifest a virulence phenotype upon AIP induction. All four *S. aureus agr* types were streaked onto 5% blood agar plates overlaid with concentrated culture supernatants. The effect of secreted exotoxins (α-, β-, and δ-hemolysins) could be visualized by a clear zone around the streak. While the zone of inhibition is clearly visible at the 10-h time point in the control assays, AIP induction (antagonist stimulus) causes a delay of 3 to 5 h in this process (Fig. 5C; see Fig. SA17 in the supplemental material). This finding is consistent with qRT-PCR data that suggest that hemolysin levels are highest at the 7-h time point. This assay suggests that cross inhibition caused by antagonist AIPs involves a similar time frame for different AIPs (corresponding to different *agr* types).

DISCUSSION

The first step in quorum sensing involving the recognition of an AIP has been demonstrated to be localized primarily in the extracellular receptor domain of the histidine kinase AgrC. The finding that AgrC is a dimer, regardless of AIP binding or phosphorylation, provided an impetus for a mechanistic model that could rationalize how differences in AIP recognition lead to differences in intracellular responses (8). The temporal fidelity of the intracellular signal transduction mechanism remains less clear. Furthermore, recent studies have revealed that other environmental triggers also influence the quorum-sensing response. For example, redox stimuli regulate AgrA activity (40) and the stability of RNAIII depends on CshA activity (41). These observations suggest that the sequence of events that precede the AgrA-induced phenotypic switch from persistent to virulent bacteria is more elaborate than hitherto anticipated. In this context, it is worth noting that phosphorylation dictates AgrA-DNA interactions (42). Phosphorylated AgrA binds the P3 promoter that governs RNAIII expression.

The crystal structure of $AgrC_{Cyto}$ provided a basis on which to model the transient step of $AgrC_{Cyto}$-$AgrA_{RR}$ interaction. This step is likely to govern the rate at which the signal information is transferred from the extracellular to the intracellular milieu. The structure of the ATP binding domain of AgrC revealed that the lid of the ATP binding pocket adopts a conformation that is distinct from that of other reported ATP binding domains, regardless of ATP binding (27). Although speculative, our suggestion is that the mobility of the ATP binding lid influences conditional kinase activity. This is also likely to contribute to the differences between constitutively active histidine kinases (31) and kinase activity triggered by environmental stimuli (8). The model of the $AgrC_{Cyto}$-AgrA complex provides a basis on which to rationalize specificity in the histidine kinase-response regulator interactions in the *agr* system. There are 16 two-component systems encoded by the chromosomal DNA of *S. aureus* (43). Strain-specific variations, in

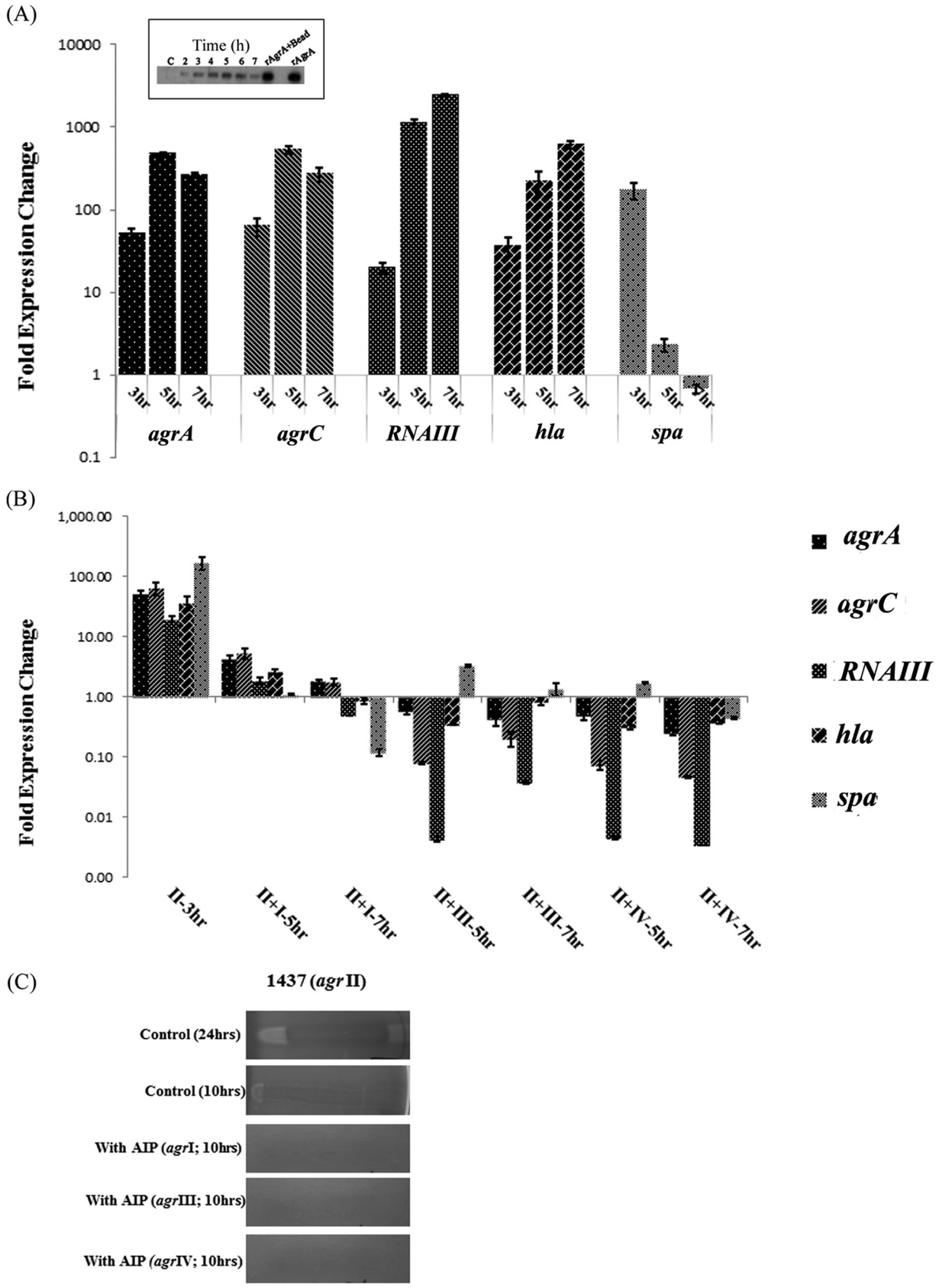

FIG 5 (A) Effects of agonistic stimuli on the transcriptional levels of genes in the *agr* regulon. *S. aureus* clinical isolate 1437 (*agr* type II) was grown at 37°C in TSB, and cells were harvested at 3, 5, and 7 h. The mRNA levels of genes in the Agr regulon (*agrA*, *agrC*, RNAIII, *hla* [α-hemolysin], and *spa* [surface protein A]) were

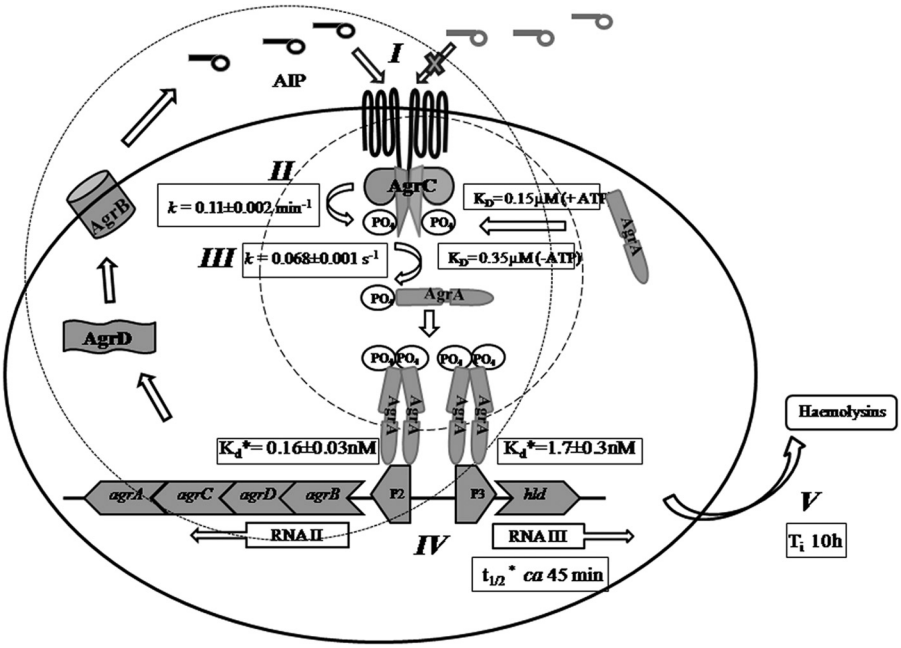

FIG 6 Schematic representation of the stages of the *S. aureus agr* quorum-sensing mechanism. This compilation, including the definition of steps I to V, is based on previous reports (8, 37, 53, 54). The focus of this study (inner dotted circle) is the intracellular signal transduction step regulated by the $AgrC_{Cyto}$-AgrA complex. The binding affinity for the $AgrC_{Cyto}$-AgrA interactions (including the effect of phosphorylation), as well as the enzyme kinetic parameters, rationalizes the spontaneity in triggering an intracellular response to an AIP stimulus. The signal amplification (larger circle) is slower, with a time frame of ca. 5 h. It is at this stage where the effect of the stability of RNAIII (half-life, >45 min [55]) is likely to be important. Our data (Fig. 5) suggest a linear AgrA concentration increase at both the mRNA and protein levels. This finding supports a mathematical model placing AgrA expression in a leading position before that of other genes in the *agr* regulon.

addition to plasmid-encoded two-component systems, are also likely, thereby increasing the number of these signal transduction modules in *S. aureus*. While we do not have comprehensive data to suggest that AgrA is the sole cognate receptor for phosphotransfer from AgrC, sequence features support specificity in AgrC-AgrA interactions. Comparisons of the sequences of AgrC and other histidine kinases and of AgrA and other response regulators in *S. aureus* suggest that sequence features are likely to enforce fidelity in kinase-response regulator interactions (33). Indeed, no interaction or phosphotransfer between $AgrC_{Cyto}$ and the two noncognate response regulators VraR and LytR was seen. A rapid phosphotransfer step is also an indicator of specificity in histidine kinase-response regulator interactions. A recent study of *Myxococcus xanthus* two-component systems demonstrated a 5,000-fold-difference between the phosphotransfer rates of cognate two-component pairs and other response regulators (32). While the phosphotransfer step between cognate histidine kinase-response regulator pairs was rapid (within 1 min) *in vitro*, nonspecific phosphotransfer was seen only upon prolonged incubation. This *in vitro* finding on the phosphorylation and phosphotransfer steps in the agr system could also form the basis for further *in vivo* analysis. Investigations of the *in vivo* biochemistry of the *E. coli* PhoB-PhoR two-component system, for example, provided a route by which to evaluate the role of histidine kinase-response regulator interactions in the fidelity of intracellular signal transduction. These studies also revealed a direct role for the binding affinity between the kinase and response regulator domains—a weaker interaction between *E. coli* PhoR and a mutant form of the response regulator PhoB could be correlated with higher, nonrobust phosphorylation (44).

The mechanistic steps involved in AIP-induced phenotypic changes are summarized in Fig. 6. The first step, i.e., recognition of AIP by the AgrC ectodomain and the subsequent transmission of this information to the catalytic histidine kinase domain, has been characterized earlier. The sensor domain of AgrC is also the least conserved in the *agr* operon across *S. aureus* strains. The intracellular components, however, reveal extensive sequence conservation. (Fig. 1C). A corollary to this observation is that the intracellular steps in signal transduction and the response time for the change in the phenotype of *S. aureus* are likely to be independent

quantified. The error bars represent standard deviations of triplicates, and fold changes in expression are on a log scale. The inset shows the immunoprecipitation of AgrA from *S. aureus* cell lysates at different time points. Freshly purified recombinant AgrA was used as the control. (B) Effect of antagonistic stimuli on the transcriptional levels of genes in the *agr* regulon. The expression of *agrA*, *agrC*, RNAIII, *hla*, and *spa* was monitored after cells were subjected to antagonistic stimuli. In this representative illustration, clinical isolate 1437 (*agr* type II) was grown until the early exponential phase (3 h). Supernatants from *S. aureus* 559 (*agr* type I), 1039 (*agr* type III), and 368 (*agr* type IV) were added to the cultures, and they were grown further before the isolation of cells at 5 and 7 h. For clarity, the *agr* types are represented as I, II, III, and IV. (C) Effects of antagonistic stimuli on hemolysis. *S. aureus* strain 1437 was streaked onto 5% blood agar plates containing AIPs of other *agr* types. The clearance zones provide a measure of hemolysis. The effect of AIPs on hemolysis was visually monitored by comparison with blood agar plates without AIPs. These findings on the effects of agonist and antagonist stimuli were consistent across all of the clinical strains examined in this study (see Fig. SA17 in the supplemental material).

of the *agr* type. Potential sources of variability, however, are the phosphorylation-induced dimerization of AgrA and the stability of this protein. These hypotheses were examined in this study. The $AgrC_{Cyto}$-AgrA interactions were experimentally examined by SPR spectroscopy (Fig. 3B and C) and fluorescence spectroscopy (Fig. 3D to F). A mechanistic interpretation was greatly aided by a model of the AgrC-AgrA complex. This model describes the first step in intracellular signal transduction (stage III in Fig. 6). We note that this interaction is dependent on the ATP concentration. That these surfaces are indeed buried upon AgrC-AgrA interactions could also be validated by fluorescence assays wherein tryptophan was used as a site-specific reporter. Despite extensive efforts, we were unable to determine the intracellular concentration of active, phosphorylated AgrA. Nevertheless, we could determine that AgrA is not degraded in the time course of the studies to evaluate AIP-induced transcriptional reengineering. The kinetics of AgrC-AgrA interactions, coupled with the poor stability of the phosphorylated Asp residue in AgrA, suggest that this step is necessarily rapid to ensure fidelity of signal transduction. The next step in the intracellular cascade involves the direct interaction of phosphorylated AgrA with promoter elements to induce or repress mRNA levels. The tight coupling of this stage with the earlier phosphotransfer step suggests that these two steps in the cascade are unlikely to differ across *S. aureus* strains.

Studies attempting to mathematically model the *agr* quorum-sensing mechanism suggest that upregulation of AgrA production is a limiting factor in ensuring that a homogeneous population of *S. aureus* cells achieves an upregulated state (45). Mathematical models of this system incorporate conditions to simulate a spatially homogeneous environment or to evaluate inhibition in a nonhomogeneous system (46, 47). One finding is that AgrA expression is present in a leading position on an earlier time scale than other proteins. While this squarely places the AgrC-AgrA complex in a controlling role, it is worth noting that the assumption of fast, switch-like behavior is an intrinsic feature of mathematical models of quorum-sensing mechanisms in general (48). Furthermore, these models describe distinct subloops (pictorially represented in Fig. 6). Jabbari and coworkers have suggested that each subloop in the quorum-sensing system is likely to play a distinct role. The upregulation of AgrA, followed by AgrC, in particular, acquires significance in a spatially homogeneous population model wherein a few cells are upregulated earlier than others (45). The data presented in this report serve to correlate these two-component system mathematical models with experimental observations. The phosphorylated response regulator, with a higher affinity for the P3 promoter, ensures temporal fidelity. Other models involve constitutive phosphorylation by kinases. Signal transduction in this case is the phosphotransfer from the response regulator to the receptor. In this case, the dephosphorylated response regulator can function as an activator (46). One factor with the potential to alter these mathematical models is that the phosphorylation cascade may vary within and between strains (49). Our studies involving analysis of the cellular concentration and stability of AgrA, qRT-PCR analysis, and estimation of the levels of secreted toxins suggest that the response time is independent of the *agr* type or the nature of the AIP stimulus. These findings suggest that variations in the response time are likely only in the case of cross talk between the *agr* signal transduction mechanism and other signaling pathways. An example of this is the regulation of AgrA activity by redox stimuli, wherein oxidized AgrA is inactive, leading to the termination of the signal transduction events initiated by AIP binding (40, 50). This feature is likely to be conserved across *S. aureus* strains because of the conservation of the disulfide-forming cysteines in AgrA. Phenotypic variations can thus be localized to the stability of RNAIII. This is governed by CshA-mediated degradation. However, the extent of the variation induced by this mechanism remains to be examined.

To summarize, the intracellular AgrC-AgrA complex determines the temporal fidelity of a transcriptional response to an AIP stimulus. This interaction, involving distinct steps of oligomerization and conformational changes, is conserved across *S. aureus* strains. Variations in the response time and extent of the cellular response can thus be attributed to environmental stimuli and the conditional stability of the effector molecule of the *agr* system, RNAIII.

ACKNOWLEDGMENTS

This work was supported in part by grants from the Department of Science and Technology, Government of India. A.F. is a DBT postdoctoral fellow and K.R. is a Senior Research Fellow of the Council for Scientific and Industrial Research.

The atomic coordinates and structure factors (PDB code 4BXI) has been deposited in the Protein Data Bank. Research Collaboratory For Structural Bioinformatics, Rutgers University New Brunswick. NJ (http://www.rcsb.org/).

REFERENCES

1. **Lowy FD.** 1998. Staphylococcus aureus infections. N. Engl. J. Med. **339:** 520–532. http://dx.doi.org/10.1056/NEJM199808203390806.
2. **Novick RP.** 2003. Autoinduction and signal transduction in the regulation of staphylococcal virulence. Mol. Microbiol. **48:**1429–1449. http://dx.doi.org/10.1046/j.1365-2958.2003.03526.x.
3. **Geisinger E, Muir TW, Novick RP.** 2009. agr receptor mutants reveal distinct modes of inhibition by staphylococcal autoinducing peptides. Proc. Natl. Acad. Sci. U. S. A. **106:**1216–1221. http://dx.doi.org/10.1073/pnas.0807760106.
4. **Boisset S, Geissmann T, Huntzinger E, Fechter P, Bendridi N, Possedko M, Chevalier C, Helfer AC, Benito Y, Jacquier A, Gaspin C, Vandenesch F, Romby P.** 2007. Staphylococcus aureus RNAIII coordinately represses the synthesis of virulence factors and the transcription regulator Rot by an antisense mechanism. Genes Dev. **21:**1353–1366. http://dx.doi.org/10.1101/gad.423507.
5. **Wang R, Braughton KR, Kretschmer D, Bach TH, Queck SY, Li M, Kennedy AD, Dorward DW, Klebanoff SJ, Peschel A, DeLeo FR, Otto M.** 2007. Identification of novel cytolytic peptides as key virulence determinants for community-associated MRSA. Nat. Med. **13:**1510–1514. http://dx.doi.org/10.1038/nm1656.
6. **Zhang L, Gray L, Novick RP, Ji G.** 2002. Transmembrane topology of AgrB, the protein involved in the post-translational modification of AgrD in Staphylococcus aureus. J. Biol. Chem. **277:**34736–34742. http://dx.doi.org/10.1074/jbc.M205367200.
7. **Lina G, Jarraud S, Ji G, Greenland T, Pedraza A, Etienne J, Novick RP, Vandenesch F.** 1998. Transmembrane topology and histidine protein kinase activity of AgrC, the agr signal receptor in Staphylococcus aureus. Mol. Microbiol. **28:**655–662. http://dx.doi.org/10.1046/j.1365-2958.1998.00830.x.
8. **George Cisar EA, Geisinger E, Muir TW, Novick RP.** 2009. Symmetric signalling within asymmetric dimers of the Staphylococcus aureus receptor histidine kinase AgrC. Mol. Microbiol. **74:**44–57. http://dx.doi.org/10.1111/j.1365-2958.2009.06849.x.
9. **Shambat S, Nadig S, Prabhakara S, Bes M, Etienne J, Arakere G.** 2012. Clonal complexes and virulence factors of Staphylococcus aureus from several cities in India. BMC Microbiol. **12:**64. http://dx.doi.org/10.1186/1471-2180-12-64.
10. **Novick RP, Ross HF, Projan SJ, Kornblum J, Kreiswirth B, Moghazeh S.** 1993. Synthesis of staphylococcal virulence factors is controlled by a regulatory RNA molecule. EMBO J. **12:**3967–3975.
11. **Gilot P, Lina G, Cochard T, Poutrel B.** 2002. Analysis of the genetic variability of genes encoding the RNA III-activating components Agr and

TRAP in a population of *Staphylococcus aureus* strains isolated from cows with mastitis. J. Clin. Microbiol. **40:**4060–4067. http://dx.doi.org/10.1128/JCM.40.11.4060-4067.2002.
12. **Foster JE, Sheng Q, McClain JR, Bures M, Nicas TI, Henry K, Winkler ME, Gilmour R.** 2004. Kinetic and mechanistic analyses of new classes of inhibitors of two-component signal transduction systems using a coupled assay containing HpkA-DrrA from Thermotoga maritima. Microbiology **150:**885–896. http://dx.doi.org/10.1099/mic.0.26824-0.
13. **Clausen VA, Bae W, Throup J, Burnham MK, Rosenberg M, Wallis NG.** 2003. Biochemical characterization of the first essential two-component signal transduction system from Staphylococcus aureus and Streptococcus pneumoniae. J. Mol. Microbiol. Biotechnol. **5:**252–260. http://dx.doi.org/10.1159/000071077.
14. **Gilles-Gonzalez MA, Gonzalez G.** 1993. Regulation of the kinase activity of heme protein FixL from the two-component system FixL/FixJ of Rhizobium meliloti. J. Biol. Chem. **268:**16293–16297.
15. **Noriega CE, Schmidt R, Gray MJ, Chen LL, Stewart V.** 2008. Autophosphorylation and dephosphorylation by soluble forms of the nitrate-responsive sensors NarX and NarQ from *Escherichia coli* K-12. J. Bacteriol. **190:**3869–3876. http://dx.doi.org/10.1128/JB.00092-08.
16. **Battye TG, Kontogiannis L, Johnson O, Powell HR, Leslie AG.** 2011. iMOSFLM: a new graphical interface for diffraction-image processing with MOSFLM. Acta Crystallogr. D Biol. Crystallogr. **67:**271–281. http://dx.doi.org/10.1107/S0907444910048675.
17. **Winn MD, Ballard CC, Cowtan KD, Dodson EJ, Emsley P, Evans PR, Keegan RM, Krissinel EB, Leslie AG, McCoy A, McNicholas SJ, Murshudov GN, Pannu NS, Potterton EA, Powell HR, Read RJ, Vagin A, Wilson KS.** 2011. Overview of the CCP4 suite and current developments. Acta Crystallogr. D Biol. Crystallogr. **67:**235–242. http://dx.doi.org/10.1107/S0907444910045749.
18. **McCoy AJ, Grosse-Kunstleve RW, Adams PD, Winn MD, Storoni LC, Read RJ.** 2007. Phaser crystallographic software. J. Appl. Crystallogr. **40:**658–674. http://dx.doi.org/10.1107/S0021889807021206.
19. **Cowtan K.** 2006. The Buccaneer software for automated model building. 1. Tracing protein chains. Acta Crystallogr. D Biol. Crystallogr. **62**(Pt 9)**:**1002–1011. http://dx.doi.org/10.1107/S0907444906022116.
20. **Murshudov GN, Skubak P, Lebedev AA, Pannu NS, Steiner RA, Nicholls RA, Winn MD, Long F, Vagin AA.** 2011. REFMAC5 for the refinement of macromolecular crystal structures. Acta Crystallogr. D Biol. Crystallogr. **67:**355–367. http://dx.doi.org/10.1107/S0907444911001314.
21. **Emsley P, Cowtan K.** 2004. Coot: model-building tools for molecular graphics. Acta Crystallogr. D Biol. Crystallogr. **60:**2126–2132. http://dx.doi.org/10.1107/S0907444904019158.
22. **Schüttelkopf AW, van Aalten DM.** 2004. PRODRG: a tool for high-throughput crystallography of protein-ligand complexes. Acta Crystallogr. D Biol. Crystallogr. **60:**1355–1363. http://dx.doi.org/10.1107/S0907444904011679.
23. **Laskowski RA, MacArthur MW, Moss DS, Thornton JM.** 1993. PROCHECK: a program to check the stereochemical quality of protein structures. J. Appl. Crystallogr. **26:**283–291. http://dx.doi.org/10.1107/S0021889892009944.
24. **Balaban N.** 2011. Isolation of agr quorum sensing autoinducers. Methods Mol. Biol. **692:**47–59. http://dx.doi.org/10.1007/978-1-60761-971-0_4.
25. **Livak KJ, Schmittgen TD.** 2001. Analysis of relative gene expression data using real-time quantitative PCR and the 2(-Delta Delta C(T)) method. Methods **25:**402–408. http://dx.doi.org/10.1006/meth.2001.1262.
26. **Sakoulas G, Eliopoulos GM, Moellering RC, Jr, Wennersten C, Venkataraman L, Novick RP, Gold HS.** 2002. Accessory gene regulator (*agr*) locus in geographically diverse *Staphylococcus aureus* isolates with reduced susceptibility to vancomycin. Antimicrob. Agents Chemother. **46:**1492–1502. http://dx.doi.org/10.1128/AAC.46.5.1492-1502.2002.
27. **Marina A, Waldburger CD, Hendrickson WA.** 2005. Structure of the entire cytoplasmic portion of a sensor histidine-kinase protein. EMBO J. **24:**4247–4259. http://dx.doi.org/10.1038/sj.emboj.7600886.
28. **Dutta R, Inouye M.** 2000. GHKL, an emergent ATPase/kinase superfamily. Trends Biochem. Sci. **25:**24–28. http://dx.doi.org/10.1016/S0968-0004(99)01503-0.
29. **Gutu AD, Wayne KJ, Sham LT, Winkler ME.** 2010. Kinetic characterization of the WalRKSpn (VicRK) two-component system of *Streptococcus pneumoniae*: dependence of WalKSpn (VicK) phosphatase activity on its PAS domain. J. Bacteriol. **192:**2346–2358. http://dx.doi.org/10.1128/JB.01690-09.
30. **Grimshaw CE, Huang S, Hanstein CG, Strauch MA, Burbulys D, Wang L, Hoch JA, Whiteley JM.** 1998. Synergistic kinetic interactions between components of the phosphorelay controlling sporulation in Bacillus subtilis. Biochemistry **37:**1365–1375. http://dx.doi.org/10.1021/bi971917m.
31. **Belcheva A, Golemi-Kotra D.** 2008. A close-up view of the VraSR two-component system. A mediator of Staphylococcus aureus response to cell wall damage. J. Biol. Chem. **283:**12354–12364. http://dx.doi.org/10.1074/jbc.M710010200.
32. **Willett JW, Tiwari N, Muller S, Hummels KR, Houtman JC, Fuentes EJ, Kirby JR.** 2013. Specificity residues determine binding affinity for two-component signal transduction systems. mBio **4**(6)**:**e00420-13. http://dx.doi.org/10.1128/mBio.00420-13.
33. **Bell CH, Porter SL, Strawson A, Stuart DI, Armitage JP.** 2010. Using structural information to change the phosphotransfer specificity of a two-component chemotaxis signalling complex. PLoS Biol. **8:**e1000306. http://dx.doi.org/10.1371/journal.pbio.1000306.
34. **Casino P, Rubio V, Marina A.** 2009. Structural insight into partner specificity and phosphoryl transfer in two-component signal transduction. Cell **139:**325–336. http://dx.doi.org/10.1016/j.cell.2009.08.032.
35. **Thoendel M, Kavanaugh JS, Flack CE, Horswill AR.** 2011. Peptide signaling in the staphylococci. Chem. Rev. **111:**117–151. http://dx.doi.org/10.1021/cr100370n.
36. **Lyskov S, Gray JJ.** 2008. The RosettaDock server for local protein-protein docking. Nucleic Acids Res. **36:**W233–W238. http://dx.doi.org/10.1093/nar/gkn216.
37. **Koenig RL, Ray JL, Maleki SJ, Smeltzer MS, Hurlburt BK.** 2004. *Staphylococcus aureus* AgrA binding to the RNAIII-*agr* regulatory region. J. Bacteriol. **186:**7549–7555. http://dx.doi.org/10.1128/JB.186.22.7549-7555.2004.
38. **Prabhakara S, Khedkar S, Loganathan RM, Chandana S, Gowda M, Arakere G, Seshasayee AS.** 2012. Draft genome sequence of *Staphylococcus aureus* 118 (ST772), a major disease clone from India. J. Bacteriol. **194:**3727–3728. http://dx.doi.org/10.1128/JB.00480-12.
39. **Vaudaux P, Francois P, Bisognano C, Kelley WL, Lew DP, Schrenzel J, Proctor RA, McNamara PJ, Peters G, Von Eiff C.** 2002. Increased expression of clumping factor and fibronectin-binding proteins by *hemB* mutants of *Staphylococcus aureus* expressing small colony variant phenotypes. Infect. Immun. **70:**5428–5437. http://dx.doi.org/10.1128/IAI.70.10.5428-5437.2002.
40. **Sun F, Liang H, Kong X, Xie S, Cho H, Deng X, Ji Q, Zhang H, Alvarez S, Hicks LM, Bae T, Luo C, Jiang H, He C.** 2012. Quorum-sensing agr mediates bacterial oxidation response via an intramolecular disulfide redox switch in the response regulator AgrA. Proc. Natl. Acad. Sci. U. S. A. **109:**9095–9100. http://dx.doi.org/10.1073/pnas.1200603109.
41. **Oun S, Redder P, Didier JP, Francois P, Corvaglia AR, Buttazzoni E, Giraud C, Girard M, Schrenzel J, Linder P.** 2013. The CshA DEAD-box RNA helicase is important for quorum sensing control in Staphylococcus aureus. RNA Biol. **10:**157–165. http://dx.doi.org/10.4161/rna.22899.
42. **Reynolds J, Wigneshweraraj S.** 2011. Molecular insights into the control of transcription initiation at the Staphylococcus aureus agr operon. J. Mol. Biol. **412:**862–881. http://dx.doi.org/10.1016/j.jmb.2011.06.018.
43. **Matsuo M, Kato F, Oogai Y, Kawai T, Sugai M, Komatsuzawa H.** 2010. Distinct two-component systems in methicillin-resistant Staphylococcus aureus can change the susceptibility to antimicrobial agents. J. Antimicrob. Chemother. **65:**1536–1537. http://dx.doi.org/10.1093/jac/dkq141.
44. **Gao R, Stock AM.** 2013. Probing kinase and phosphatase activities of two-component systems in vivo with concentration-dependent phosphorylation profiling. Proc. Natl. Acad. Sci. U. S. A. **110:**672–677. http://dx.doi.org/10.1073/pnas.1214587110.
45. **Jabbari S, King JR, Williams P.** 2010. A mathematical investigation of the effects of inhibitor therapy on three putative phosphorylation cascades governing the two-component system of the agr operon. Math. Biosci. **225:**115–131. http://dx.doi.org/10.1016/j.mbs.2010.03.001.
46. **Jabbari S, King JR, Williams P.** 2012. Cross-strain quorum sensing inhibition by Staphylococcus aureus. Part 1: a spatially homogeneous model. Bull. Math. Biol. **74:**1292–1325. http://dx.doi.org/10.1007/s11538-011-9701-1.
47. **Jabbari S, King JR, Williams P.** 2012. Cross-strain quorum sensing inhibition by Staphylococcus aureus. Part 2: a spatially inhomogeneous model. Bull. Math. Biol. **74:**1326–1353. http://dx.doi.org/10.1007/s11538-011-9702-0.
48. **Ji G, Beavis RC, Novick RP.** 1995. Cell density control of staphylococcal virulence mediated by an octapeptide pheromone. Proc. Natl. Acad. Sci. U. S. A. **92:**12055–12059. http://dx.doi.org/10.1073/pnas.92.26.12055.
49. **Wuster A, Babu MM.** 2008. Conservation and evolutionary dynamics of

the *agr* cell-to-cell communication system across firmicutes. J. Bacteriol. **190:**743–746. http://dx.doi.org/10.1128/JB.01135-07.
50. **Roux A, Todd DA, Velazquez JV, Cech NB, Sonenshein AL.** 2014. CodY-mediated regulation of the *Staphylococcus aureus* Agr system integrates nutritional and population density signals. J. Bacteriol. **196:**1184–1196. http://dx.doi.org/10.1128/JB.00128-13.
51. **Wu S, Zhang Y.** 2007. LOMETS: a local meta-threading-server for protein structure prediction. Nucleic Acids Res. **35:**3375–3382. http://dx.doi.org/10.1093/nar/gkm251.
52. **Landau M, Mayrose I, Rosenberg Y, Glaser F, Martz E, Pupko T, Ben-Tal N.** 2005. ConSurf 2005: the projection of evolutionary conservation scores of residues on protein structures. Nucleic Acids Res. **33:**W299–W302. http://dx.doi.org/10.1093/nar/gki370.
53. **Janzon L, Arvidson S.** 1990. The role of the delta-lysin gene (hld) in the regulation of virulence genes by the accessory gene regulator (agr) in Staphylococcus aureus. EMBO J. **9:**1391–1399.
54. **Ji G, Beavis R, Novick RP.** 1997. Bacterial interference caused by autoinducing peptide variants. Science **276:**2027–2030. http://dx.doi.org/10.1126/science.276.5321.2027.
55. **Huntzinger E, Boisset S, Saveanu C, Benito Y, Geissmann T, Namane A, Lina G, Etienne J, Ehresmann B, Ehresmann C, Jacquier A, Vandenesch F, Romby P.** 2005. Staphylococcus aureus RNAIII and the endoribonuclease III coordinately regulate spa gene expression. EMBO J. **24:**824–835. http://dx.doi.org/10.1038/sj.emboj.7600572.
56. **Kelly LA, Sternberg MJE.** 2009. Protein structure prediction on the web: a case study using the Phyre server. Nat. Protoc. **4:**363–371. http://dx.doi.org/10.1038/nprot.2009.2.